AIAA SciTech
5-9 January 2015, Kissimmee, Florida
53rd AIAA Aerospace Sciences Meeting

Fluid-Structure Interaction of a Variable Camber Compliant Wing

Samuel C. Miller *
Air Force Research Laboratory, Wright-Patterson AFB, Ohio, 45433, USA
Markus P. Rumpfkeil †
University of Dayton, Dayton, OH, 45469, USA
James J. Joo‡
Air Force Research Laboratory, Wright-Patterson AFB, Ohio, 45433, USA

This paper presents results for a loosely-coupled fluid-structure interaction (FSI) of a flexible wing using FUN3D to compute the aerodynamic flow-field and Abaqus to calculate the structural deformation. NASA Langley also provides a general 3D algorithm to interpolate between dissimilar meshes which is used here to map pressures and displacements between the aerodynamic and structural codes. This method is applied to the AFRL - developed "Variable Camber Compliant Wing" (VCCW), which is an adaptable wing designed target airfoil shapes between a NACA 2410 and 8410. Results will be compared to experiments conducted in the AFRL Vertical Wind Tunnel.

I. Introduction and Motivation

Fluid-structure interaction (FSI) can be defined as the phenomena where the interface between a structure and the surrounding fluid have a coupled relationship. Examples in nature can be found in arterial blood flow, aeroelastic effects in aircraft, and architectural responses to wind forces. The study of FSI is of particular importance for aerospace applications where aerodynamic forces cause structural motion, such as aeroelastic flutter or even significant and sustained deformation. Oscillatory effects such as flutter can cause serious structural fatigue and a lack of adequate stability and control power. In the past, aeroelastics have been an afterthought when applied to aircraft design, but as the aerospace industry moves towards an increased use of composites, this will also greatly increase the need to study the interaction between flexible structures and their aerodynamics during the design process. Incorporating FSI analysis into the design process will facilitate this development and eventually help to improve efficiency and to optimize the design. The Air Force Research Laboratory (AFRL) has developed a novel adaptive Variable Camber Compliant Wing[1](VCCW) that can actively change camber by using a compliant mechanism. The goal of the design is to create a distributed camber control capable of reconfiguration through continuous deformations to optimize its shape to suit its current altitude, airspeed, and lift-to-drag (L/D) ratio requirements. Detrimental aerodynamic conditions such as separated flow and increased parasitic drag, caused by gaps and holes from traditional control surfaces, are avoided by the seamless construction of the VCCW. Due to the significant coupling between the structural and aerodynamic domains unique to its design, the VCCW provides the perfect test case for a fluid-structure interaction analysis.

*Graduate Student, Dept. of Mechanical and Aerospace Eng., millers23@udayton.edu, Student Member AIAA.
†Assistant Professor, Dept. of Mechanical and Aerospace Eng., Markus.Rumpfkeil@udayton.edu, Senior Member AIAA.
‡Research Mechanical Engineer, AFRL/RQVC,James.Joo.1@us.af.mil, Senior Member AIAA

II. FSI Architecture

II.A. Loosely-Coupled Approach

There are two different fundamental ways to conduct FSI simulations: Tightly or loosely coupled. Tightly-coupled, or monolithic, techniques require access to both the fluid and the structural solver source codes in order to enable the solution of both systems of equations simultaneously. The loosely coupled approach, further categorized as explicit, implicit, or semi-implicit, treats both the fluid and structure codes separately and solves the systems of equations independent of each another. Both coupling techniques have advantages and disadvantages depending on the particular problem and availability of source code. Loosely-coupled methods often suffer from lack of sufficient time-accuracy and numerical stability compared to tightly-coupled approaches, and their computational efficiency has been debated.[2] However, they do have the advantage of easier software integration and modularity and are less computationally expensive per time step. For large, complex problems, separate, highly specialized solvers are often better suited to solve the individual problems due to the inherent nature of the mathematics involved.[3] Due to the fact that the structural solver used in the design and analysis of the VCCW was commercial, a loosely coupled approach was chosen.

The aerodynamic flow solution, in the form of the vector y in Eq. (1), denotes the pressure distribution on the aeroelastic body within the fluid domain. The initial aerodynamic flow-field solution is obtained on the non-deformed geometry. Once the flow-field is established and converged, the aeroelastic body deformation is determined by the separate structural solver. The CFD mesh is then adapted to match the shape of the new deformed body as defined by the structural code. The flow solution is then restarted and updated based on the new geometry. Once the updated solution is obtained, the new pressure distribution along the surface is exported to the structural solver.

$$y^{n+1} = F(x^n) \tag{1}$$

The structural deformation solution, given as the vector x in Eq. (2), denotes the displacements of each node of the aeroelastic body, based on the fluid-structure interface. The surface pressures defined by the flow solution are imported as a mapped, distributed load on the structure. Once the new deformations are obtained, they are exported to the flow solver for an updated surface pressure distribution.

$$x^{n+1} = S(y^{n+1}) \tag{2}$$

This method is referred to as a conventional serial staggered (CSS) scheme[3,4] and is detailed in Table 1 and Figure 1. This approach is only first-order time accurate, but has been found to be suitable for aeroelastic simulations[2,3,5–7] where n serves simply as an iteration or time-step counter. Note that this paper only addresses the steady-state aerodynamic and structural responses.

Table 1. Conventional Serial Staggered Scheme

Solve flow equations	$y^{n+1} = F(x^n)$
Solve structural equations	$x^{n+1} = S(y^{n+1})$
Increment to next step	

II.B. Software

Getting the two solvers to communicate with each other was fairly straight forward from a computer science perspective. The crucial step in the loosely coupled method is during the interpolation of solutions between the two different solvers. CFD and FEA meshes typically have significantly different resolutions that require a careful mapping between them.

FUN3D,[8] which is developed and maintained by the NASA Langley Research Center, was the CFD solver used. It is an unstructured, Reynolds Averaged Navier-Stokes (RANS), finite volume CFD solver. FUN3D can support steady or time-dependent simulations, with moving, adaptable, and overset grids, design optimization, and adjoint-based error estimation. The external aeroelastic module built into FUN3D allowed boundary surfaces to be imported and exported into the volume mesh. At the conclusion of each CFD run, the boundary surface was exported in a format specifically designed to be sent to the interpolation code used to map between FEA and CFD.

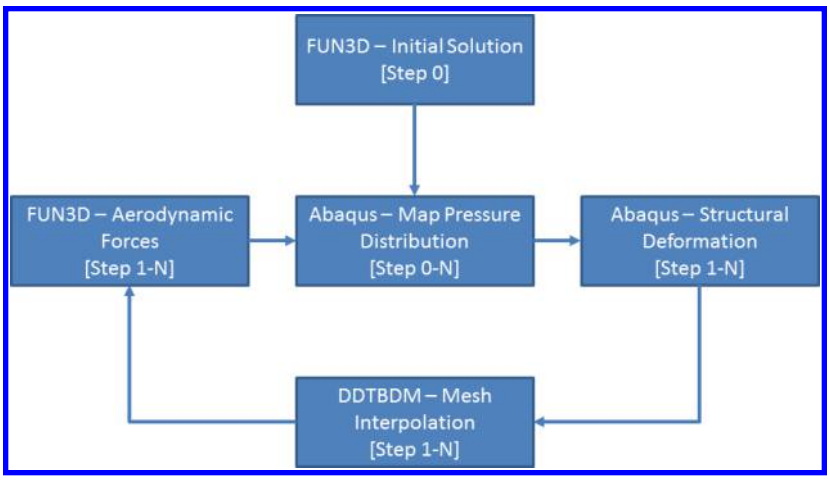

Figure 1. Loosely-Coupled Approach

Abaqus, a commercially available finite element analysis software suite, was used to create and analyze the structural response of the compliant wing under deformation due to actuation and aerodynamic loading. Abaqus includes Python modules which allowed detailed access to the structural model and results. Extensive scripting was used to parse the output, create displacement and model definition files, and pass the data to the mesh interpolation code.

Samareh[9,10] provides a general 3D algorithm to facilitate transfers between different meshes in various formats. This software, DDTBDM (Discrete Data Transfer Between Dissimilar Meshes), handles the transfer of displacement outputs given by Abaqus onto the aeroelastic surface output given by FUN3D. This mapped CFD mesh is then sent back to FUN3D as a deformed surface. The data transfer is accomplished in three steps: 1) find the nearest source element for every target point, 2) calculate the mapping coefficients for every target point and its corresponding (nearest) source element, and 3) interpolate/inject from the source element to the corresponding target point.

Python was used extensively to manage the communication between the three separate codes. It facilitated automatic monitoring of solutions, file format management and conversions, as well as local and remote server job submission. A object-oriented approach was taken to allow future applications to generic fluid-structure interaction problems.

III. Variable Camber Compliant Wing

AFRL built and tested two versions of the Variable Camber Compliant Wing; a 1 ft (0.3 m) bench-top model used to test the compliant mechanism, and a second 6 ft model for testing under full aerodynamic loads in a wind tunnel. The 6 ft prototype is a straight, uniform, rectangular wing with a 6 ft (1.8 m) span and 2 ft (0.61 m) chord. The objective of the VCCW's design was to achieve a six percent change in maximum camber with standard NACA four digit series profiles as the target (NACA 2410 through 8410). A single force actuation was designed to continuously change the camber through the embedded compliant mechanism. During actuation, the leading and trailing edges travel vertically with respect to the constant camber location at the spar. Due to its camber changes and flexible nature, the VCCW provided a unique problem set and was an ideal candidate for a fluid-structure interaction analysis.

III.A. Experimental Testing

The main objective of the wind tunnel test was to demonstrate the response of the VCCW under aerodynamic load through skin deflections and the resulting lift and drag response. The Vertical Wind Tunnel (VWT) facility at Wright-Patterson Air Force Base was chosen because of the available flow regime and physical accessibility to the model. The VWT has a 12 ft (3.66 m212) diameter, open-jet test section that can offer flow speeds up to 150 ft/s (46 m/s). The open test section allowed for the installation of optical measurement equipment, light sources, and other equipment that was used to perform surface oil-flow visualization and digital image correlation. Since the wing was smaller than the test section, a custom fixture had to be

designed to support the model as well as measure forces and moments. An in-depth discussion of the wind tunnel and the testing procedures is detailed in the paper by Marks et al.[11] Force and moment data, and the resulting lift and drag acquired by the force couples embedded in the support structure, is not included in the analysis presented here. Fixture alignment issues and other unknowns will require further analysis to be fully understood. Local section lift coefficients were calculated by surface static pressure taps located near the mid-span of the wing. The test matrix is summarized in Table 2 below. Note the depiction of the wind tunnel test configuration in Figure 2(a) and a sample of the flow visualization completed during the test in Figure 2(b).

Table 2. Experimental Test Configuration

Freestream Velocity	50 knots (25.7 m/s)
Reynolds number	1.05 x 10^6
Mach	0.076
Chord	2 ft (0.61 m)
Span	6 ft (1.8 m)
Wetted Area	12 ft^2 (1.12 m^2)
Angle of Attack	-4 to 8 degrees
Target NACA Camber	2410, 3410, 4410, 6410, 8410

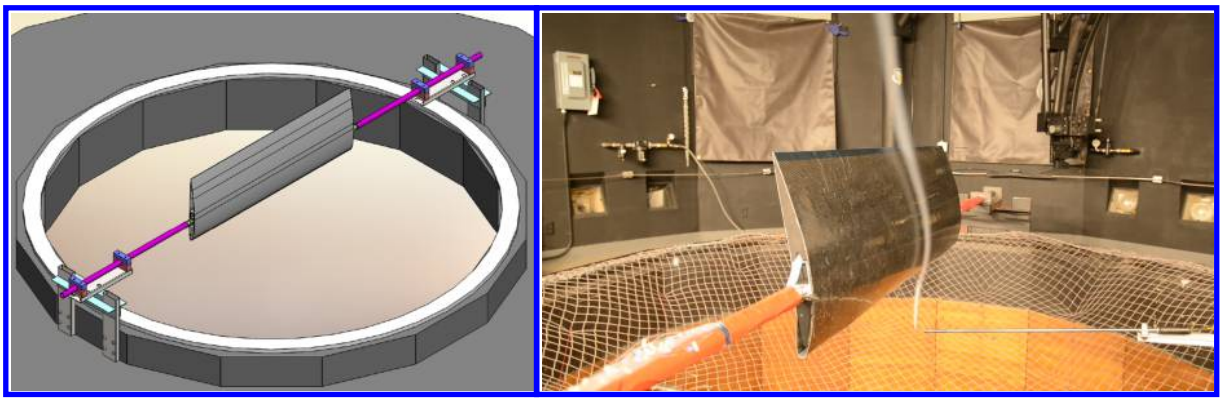

(a) Tunnel Configuration (b) Flow Visualization

Figure 2. 6 ft VCCW model installed in the WPAFB Vertical Wind Tunnel

III.B. Finite Element Analysis

The FEA model used for this project was previously built for the stress analysis and design phase of the VCCW project. For the FSI analysis, this model was used as the baseline and was modified to facilitate communication between the FEA and CFD codes. The model itself was constructed of aluminum, composites, and 3D additive materials. Its complex internal structure is beyond the scope of this paper. The specific design of the model is covered more in two companion papers.[1,11] The flexible composite material, used to allow the high range of motion during camber changes, proved to be difficult to model within FEA and was the limiting factor in this analysis.

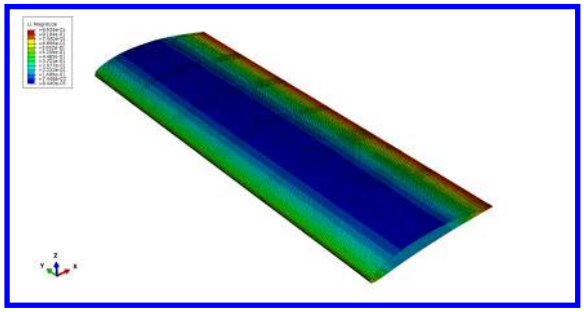

Figure 3. Abaqus FEA mesh configuration

A 1 ft version FEA model was built to verify the desired shapes, and while this particular FEA model did not include all of the skin material, it was still able to match the desired camber shapes. This model used a uniform 2D pressure distribution imported from XFOIL, and was deemed sufficient for the purpose

of maximum stress/strain testing purposes. Both versions of the model were constrained by fixing each spar end. The remainder of the model was allowed to flex. An additional full-scale 6 ft model was also built in Abaqus to test the support fixture and overall structural response of the full model under a static 2D uniform load. The primary intent of this model was to ensure support structure integrity during a wind tunnel test. The analysis presented in this paper only shows the results from the 6 ft FEA model without the support structure. Future work could increase the fidelity of the analysis by including the support structure, which would show additional bending along the span. Due to the vertical arrangement of the tunnel, gravity could also be included to account for the model bending under its own weight.

The FEA model was modified to only output the new deformed shape once the camber change and skin deflections had been computed. Neither the FEA model nor the physical wing had caps at the end, leaving it open to air flow. The wind tunnel model had foam, shown in Figure 2(b), inserted into the end sections to close off the majority of the sides. The CFD analysis requires a closed model, so caps were added to that specific mesh. Material test data was taken on a specimen of the skin, but the results were highly variable and only served to get a baseline estimate for the material model within Abaqus. The selection of the compliant composite material model significantly impacted the deformation response, and ultimately the overall FSI answer. Further work on the VCCW computational analysis is needed to determine the best material model to use.

One of the unique challenges associated with this project was determining the actual shape of the physical model while in the wind tunnel. Laser scans of the physical model were taken at each camber configuration. These provided extremely high resolution triangular meshes which were used to extract the airfoil profiles along the span. These profiles were used as reference positions in order to match the actuated FEA model with the test shape in the wind tunnel. This meant that the ideal NACA profiles were only used as a baseline estimate; the actual profile scans were quite a bit different, particularly at the leading edge. In order to match the test conditions closely, the FEA model had to first actuate to the correct estimated camber prior to turning on the aerodynamic loads.

Run-times for the FEA models were significantly less than the CFD simulations, as expected. The FEA model had 112,000 nodes and 110,000 quadrilaterals and tetrahedral elements. The initial FEA solution took roughly 20-30 minutes on six Intel Xeon cores and restarted solutions took about 5-10 minutes each, depending on the angle of attack and camber. Higher camber cases took longer to run due to the increased level of deformation within the FEA model.

III.C. Computational Fluid Dynamics

The CFD model was a simple, rectangular, 6 ft wing in free-space with no tunnel or support structure interference and the flow was assumed to be steady-state. While not ideal, due to the fact that even the center-line of the wing will most likely not be symmetric because of the wing tip vortex interaction, this configuration captured enough of the physics to get a basic flow-field established and to capture wing tip effects. The interference effect of the support structure was not included in the initial analysis, but has a definitive physical interaction that cannot be completely neglected, particularly in future work.

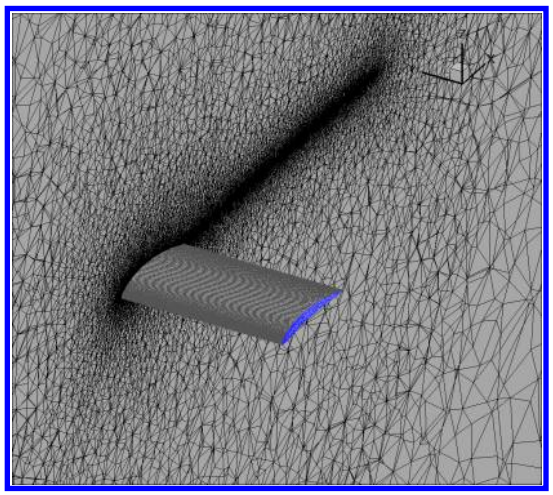

Figure 4. CFD mesh configuration (slice at 50 percent span)

In terms of the predictions of deformation and lift, the interference effect caused by the support structure manifests itself as noise data along the wing tips. Any time-dependent effects are averaged out due to the nature of RANS CFD. The primary mesh used was a 3D unstructured tetrahedral mesh that contained 2.77 million nodes. A view of the wing boundary surface mesh as well as a slice down the center of the volume is shown in Figure 4. A mesh resolution study was performed on the lift and drag coefficients at the same configuration of the wind tunnel test with medium and fine meshes containing 11.9 and 49 million nodes respectively. A comparison was done at angles of attack from -4 through 6 degrees, in 2 degree increments, at an airspeed of 50 knots and a Reynolds number of 1.05 x 10^6. The results from this study can be seen in Figures 5(a) through 5(d).

For the FSI analysis, the same initial mesh and solution was used for every case at the respective angle of attack, which consisted of the ideal NACA 2410 finite wing. Any deformations and camber changes were due to the solution obtained by the FEA solver Abaqus. The cases were all run second-order accurate in space with the Spalart-Allmaras[12] turbulence model and an average y-plus value of less than one. CFD run-times for the baseline mesh were 1 hour on 240 Intel Xeon X560 cores for the initial solution and approximately 30 minutes on 120 Intel Xeon X560 cores for each restart. The initial solutions on the medium and fine mesh took 4.5 and 20 hours, respectively, using the same hardware configuration.

Considerable time was spent building the mesh to allow proper mesh deformation, particularly for cases with large changes in camber. The employed mesh was fully 3D with no symmetry planes, and required careful attention to the mesh topology around the wing-tips and end-caps. The topology of the wing caps changes considerably between a NACA 2410 and 8410, and the sharp edges along the caps were difficult to mesh. This ultimately drove the decision to use an unstructured tetrahedrally dominated mesh. FUN3D also contains additional mesh deformation utilities specifically for fixing tangled tetrahedrals during the deformation stage. Creating the right mesh to work for this problem became more of an art than science. Once a mesh was found to deform well in all cases, the configuration was frozen and used throughout the test matrix.

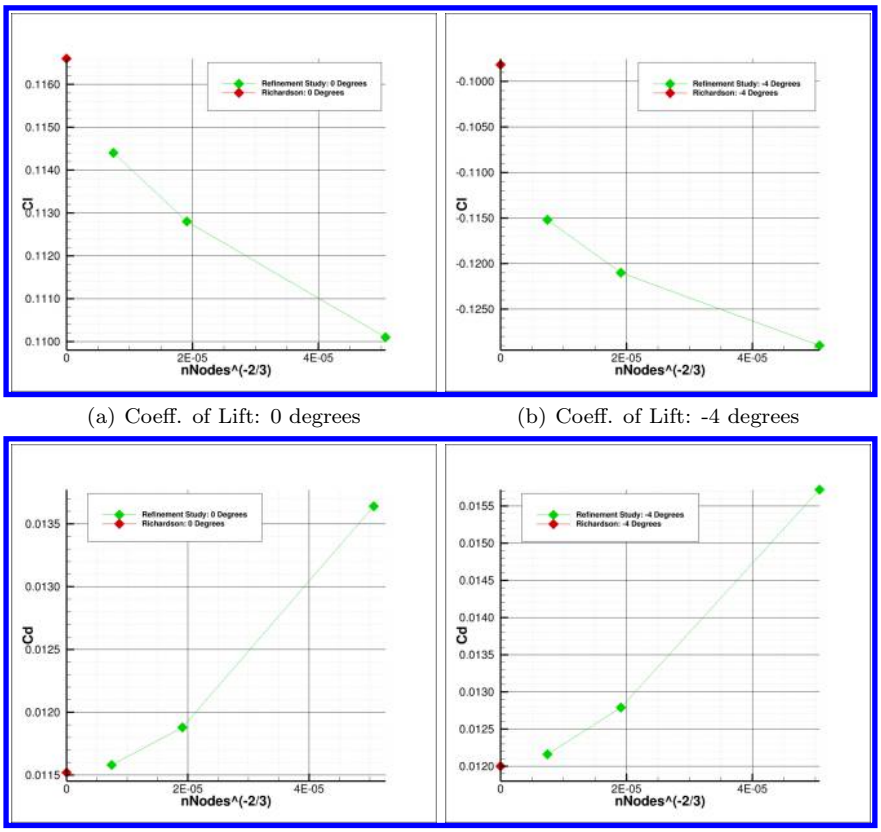

(a) Coeff. of Lift: 0 degrees (b) Coeff. of Lift: -4 degrees

(c) Coeff. of Drag: 0 degrees (d) Coeff. of Drag: -4 degrees

Figure 5. CFD Mesh Resolution Study: Initial FSI configuration (NACA 2410)

The external aeroelastic routine in FUN3D exports specified boundary surfaces at desired iteration increments. These exported boundary surfaces contain the force data needed to interpolate to a separate structural solver. Once the new shape was found by the FEA model, the newly deformed surface shape was inserted in place of the prior boundary surface as long as the same mesh structure was observed (same number of nodes and cells). Each FSI simulation started with the rigid model in a steady CFD simulation with the established flow-field. Each subsequent FSI iteration took significantly less time than the very first iteration due to the fact that the previous solution is a pretty good initial guess. Figure 6 shows the differences in the convergence history between cases with no change and large camber changes. After the first two or three FSI iterations the lift and drag coefficient stop changing significantly in all cases.

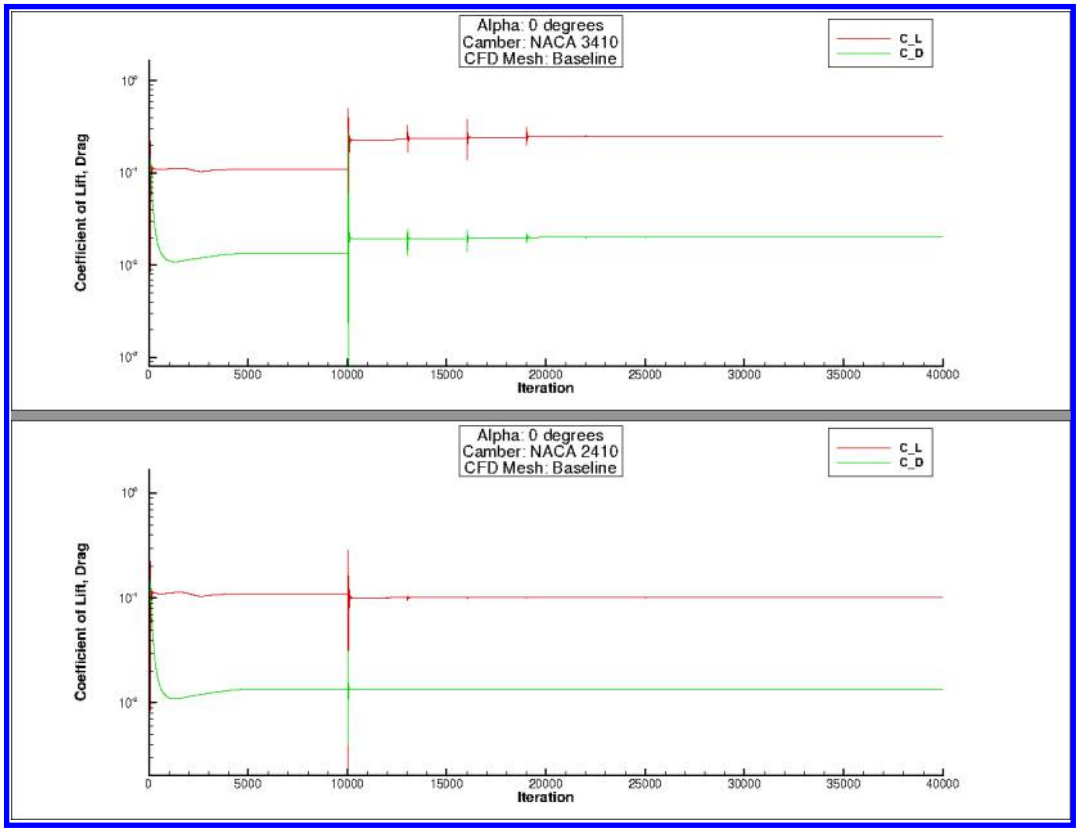

(a) Lift/Drag History

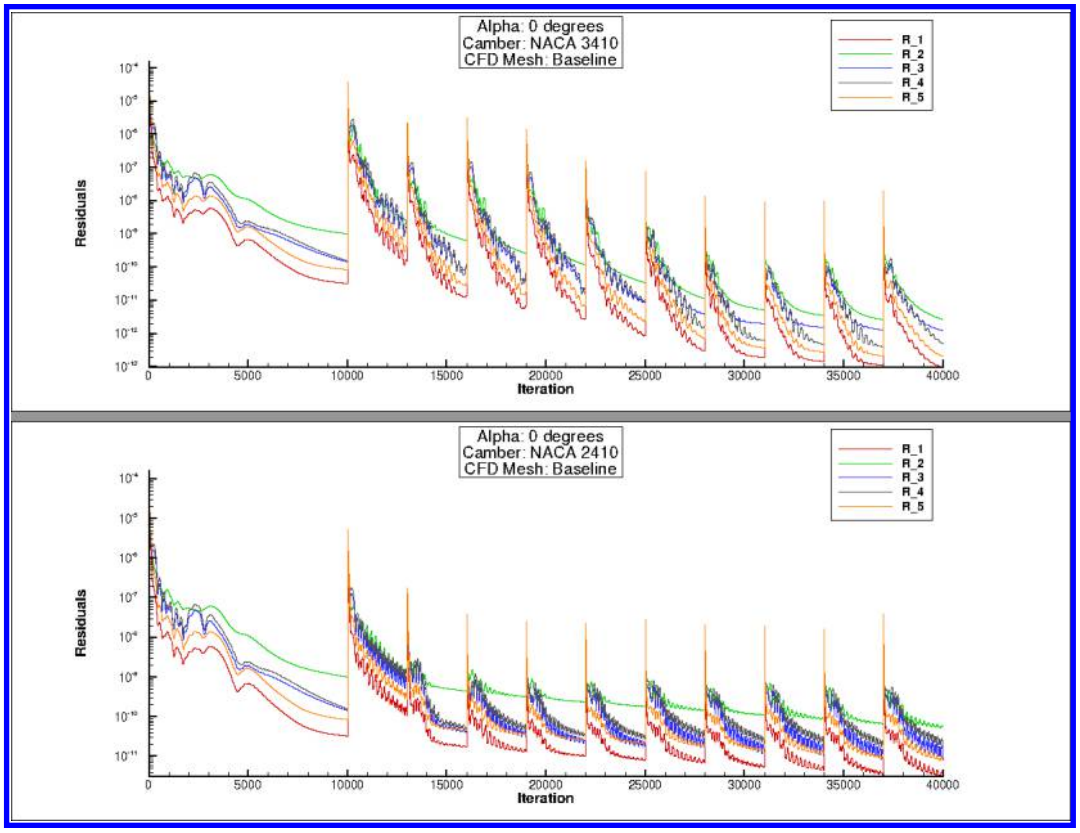

(b) CFD Residual History

Figure 6. CFD convergence history for the NACA 3410 (top) and 2410 (bottom) cambers at 0 degrees

IV. Results

One of the major unknowns at the beginning of this project was the criteria needed to determine convergence for the fluid-structure interaction analysis. At a first glance, one might think that convergence is reached once the structure stops moving or is steadily oscillating about a point. For CFD solvers, though lift and drag may stop changing significantly after a point, the residuals of the governing equations will probably still change. Similarly, FEA solvers converge based on stress, strains, and displacements. Each respective solver may converge on its own, but, when coupled together, it may not result in a converged answer. In this analysis of the VCCW, output from each solver was observed to determine the combined effect.

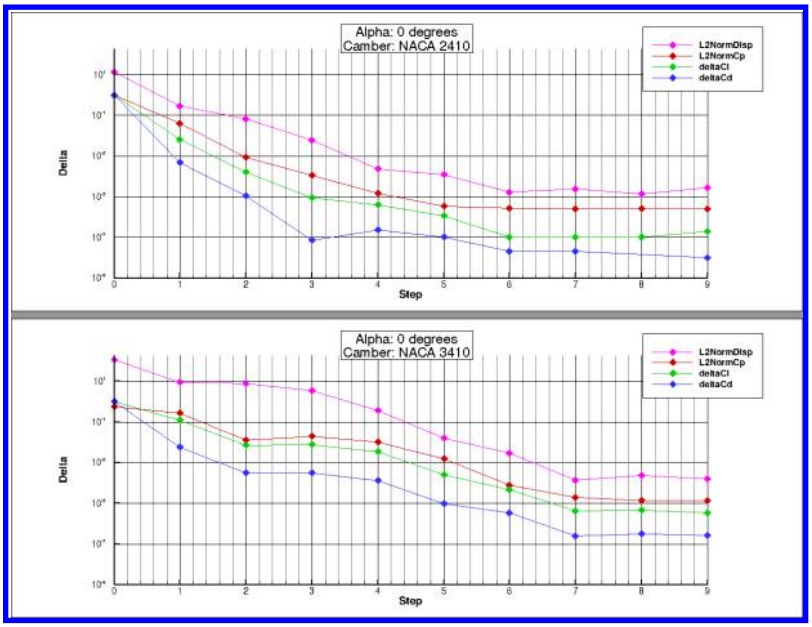

(a) Influence of camber

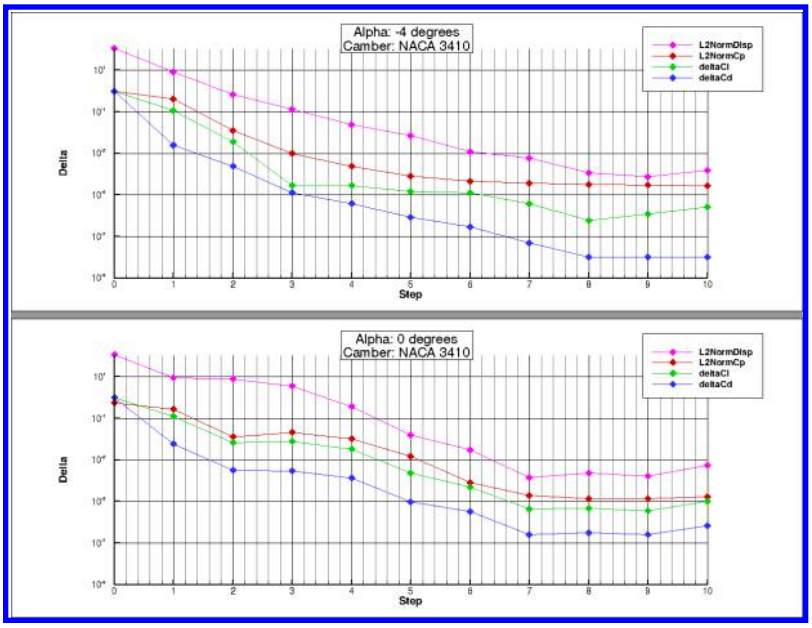

(b) Influence of alpha

Figure 7. FSI convergence history for the NACA 2410 and NACA 3410

Thus, a series of norms were taken on both the structural displacements and pressure distribution. Figure 7 shows the changes in some of these norms as well as the differences in the lift and drag coefficients between each FSI iteration. The change in the L2 norms of the displacement vectors and pressure coefficient

distribution are shown in pink and red while the green and blue lines represent the changes in the lift and drag coefficients, respectively. Figure 7(a) shows the effect of camber changes in the residuals and Figure 7(b) shows the comparison between 0 and -4 degrees angle of attack. Note the influence of camber on the rate of convergence. The FEA solver must deflect the initial shape to the desired shape first, before the updated CFD solution can be run. This is reflected in the overall FSI convergence history: the rate of convergence is delayed because of the higher level of deformation caused by the camber change. Similarly, Figure 6 shows the CFD residual history; the residual spikes indicate where the new, deformed boundary surfaces are inserted into the solution. Note that the values of lift and drag flat-line after a few steps, while the conserved variables continue to reduce. This figure shows the absolute values of lift and drag as opposed to Figure 7 which shows the change between each iteration.

Digital image correlation (DIC) data was taken for a subset of the test matrix in the wind tunnel test. This provided before-and-after images of the top surface of the wing with the air turned on and off. The DIC system took a series of snapshots with the air off to calibrate for the zero deflection state. After that, a single image was taken with the air on, giving total displacements in 3D space. Unfortunately, due to the physical restraints of the wind tunnel test section size, images were only available of the top surface, leaving the leading edge and lower surface unobserved. These 3D surfaces were processed and aligned to provide the closest one-to-one comparison of wind tunnel to FSI results. The raw surface DIC data can be seen in Figure 8(a) for each camber configuration at 0 degrees angle of attack. Since there was no easy datum to choose on this flexible wing, each surface was overlaid in order to find a common region between cambers. This location turned out to be the spar and can be easily seen in Figure 8(a). This location was chosen to align the DIC and FSI data sets. The width of the DIC data did not extend to the full width of the wing, so the center span was chosen to align experimental and simulated results.

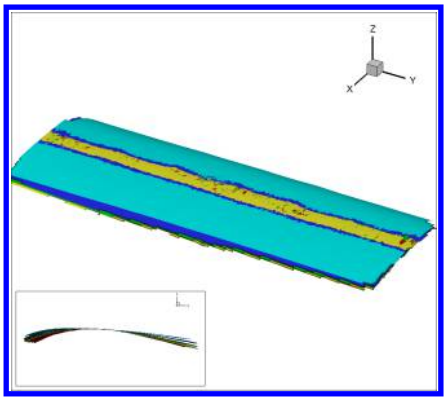

(a) Raw DIC data surfaces for 4 cambers at 0 degrees angle of attack

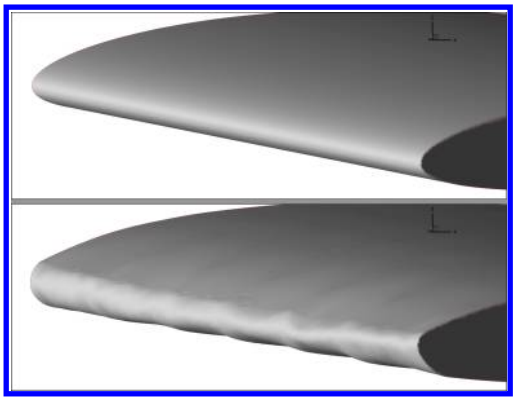

(b) Initial FSI Mesh (top) vs. Laser Scan Surface Mesh (bottom) for NACA 3410

Figure 8. Surface mesh comparisons

There were a fair amount of local twist, alignment, and uniformity issues in the fabricated model. Due to the rapid prototype nature of the model, this was expected to some extent. The inherent nature of composites and the method of construction led to this behavior and made it difficult to get the ideal NACA profiles. The biggest challenge with simulating, testing, and analyzing the VCCW was the lack of knowledge about the specific shape, regarding camber and angle of attack, of the model in the tunnel. While the laser scans of each camber configuration provided the best baseline estimate, they were taken outside of the tunnel. Since the VCCW flexes under its own weight, the repeatability of the surface shape between the laser scan and tunnel configuration is questionable. Unfortunately, only separate pieces of information were available at each point. The separate data from the laser scans and DIC surfaces were then combined to estimate the actual shape of the model. The difference in initial surface shapes between ideal and actual means that the final displacements of the FSI simulations are more likely to match in trend rather than absolute value. The non-uniformity of the prototype changes the aerodynamics, due to localized flow transition and separation from surface imperfections, and these aerodynamics combined with the disparities between the FEA material models and the true material properties ultimately change the structural response. Figure 9 shows different subsets of the displacement comparison data. Figures 9(a) and 9(b) show a span-wise slice from the wing at 96 percent chord comparing the effect of angle of attack. These show the progression of the trailing edge deflection, at the initial NACA 3410 camber, as the FSI simulation marches toward a final solution, coded

by color, from black to blue. Figure 9(c) compares the deflection of the NACA 3410 FSI and DIC results at 80 percent chord: Note the twin y-axis and that the results were not scaled, only translated to demonstrate that *the magnitudes do not match, but the behavior is similar*. The overall displacements for this case, and most others, under-predicts compared to the experiment. Note that, in the figure, the light green line shows both the upper and lower surface displacements, but the experimental results in red are only for the top surface. The displacement trends are similar, specifically the behavior at and between the ribs, along the centerline of the span. The displacement is considerably different at the tips due to the wing-tip vortex interaction and support structure interference effects neglected in this analysis.

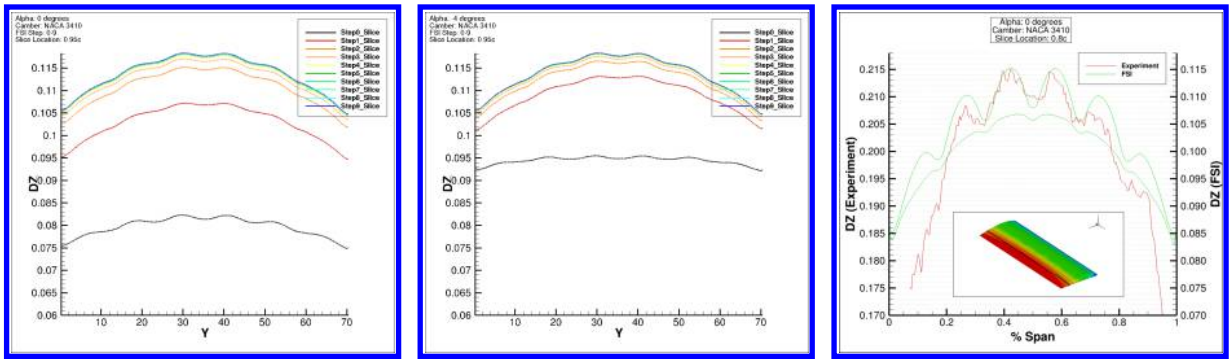

(a) NACA 3410, Alpha = 0; Span-wise slice at .95c

(b) NACA 3410, Alpha = -4; Span-wise slice at .95c

(c) Displacement Trend Comparison (NACA 3410); Span-wise slice at .8c

Figure 9. Displacement Comparisons

The coupled nature of the physical problem means that the choices of CFD and FEA configurations on their own, as well as the effect of the coupled model as a whole, impact the final result. Figure 10(a) shows how the CFD mesh resolution changes the FSI results. This figure compares the same camber (NACA 3410), alpha (-4 degrees), and FEA mesh, with two different CFD mesh resolutions (baseline and medium). The medium resolution mesh does a better capturing the finite wing effects as well as the overall lift distribution, as shown by the increased deflection of the trailing edge. As mentioned in the FEA modeling section, the choice of material models was a point of great difficulty and one that still needs to be further investigated, due to the complexity of the materials involved. At the time of this paper, the two FEA configurations that were run included a model without the leading edge material and one with a best estimated model. Multiple test specimens were taken of the leading edge material, but the variation between them suggested a highly non-linear material that was difficult to model in Abaqus. Figure 10(b) shows how much the material choice affects the end result.

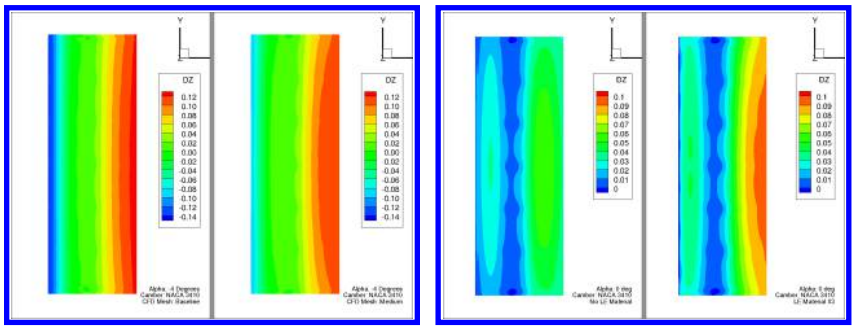

(a) CFD Mesh Effects
(L: Baseline, R: Medium)

(b) FEA LE Material Effects

Figure 10. CFD/FEA configuration effects

Because of the complexities of the structure and the resulting aerodynamic interactions, the best one-to-one comparisons between test and model data are the upper surface deflections. The subset of the results obtained are shown in Figures 11 and 12. These figures show the displacements in the z-direction, or normal to the plane of the wing. The contour levels are matched to show direct comparison. The general trends between the different angles of attack show that the trailing edge deflects the most, as expected, and that the actuation to camber effectively stiffens the structure of the wing. As mentioned earlier, the FSI results trend towards under-predicting the deflections, but still capture the same behavior. The VCCW tends to deflect

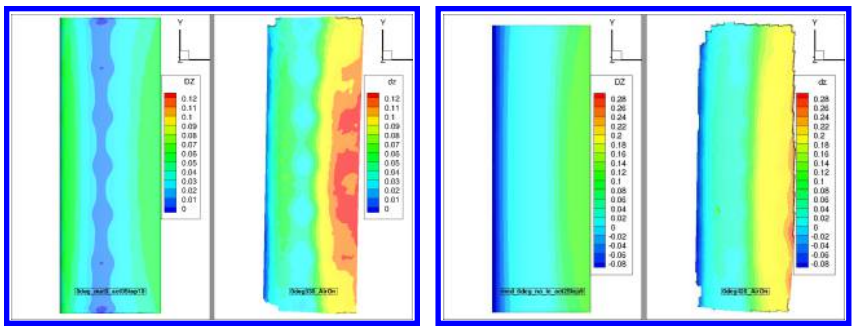

(a) NACA 2410 (L: FSI, R: DIC) (b) NACA 3410 (L: FSI, R: DIC)

Figure 11. Upper Surface Deflection Comparison: 0 degrees angle of attack

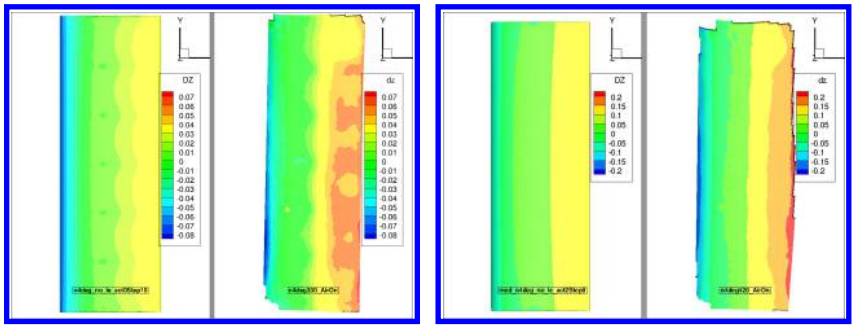

(a) NACA 2410 (L: FSI, R: DIC) (b) NACA 3410 (L: FSI, R: DIC)

Figure 12. Upper Surface Deflection Comparison: -4 degrees angle of attack

in the direction of the lift, or as a result of the combined suction/pressure. Future work will need to focus on the resulting lift and drag over the range of angles of attack in order to be able to draw better conclusions about the lift and drag performance of the flexible structure. The CFD resolution study showed higher lift as the resolution increases, and the CFD mesh effects in Figure 10(a) showed an increase in deflections as well, due to the higher lift. Figures 11 and 12 show that the FSI consistently under-predicts the trailing edge deflection in all the cases.

V. Conclusion

This paper presents loosely-coupled fluid-structure interaction (FSI) simulations using FUN3D to compute the aerodynamic flow-field and Abaqus to calculate the structural deformation of a flexible wing. NASA Langley provides a general 3D algorithm to interpolate between dissimilar meshes which serves to map pressures and displacements between the aerodynamic and structural codes. This method is applied to the AFRL - developed "Variable Camber Compliant Wing" (VCCW), which is an adaptable wing designed for active wing camber change without discrete control surfaces. Results were compared to wind tunnel test data that included digital image correlation data for surface displacements. Though the FSI method under-predicted the results when compared to the VCCW test data, overall deflection trends matched well. Higher resolution CFD and FEA modeling is suggested to improve the prediction results. Further work is also needed to refine the fidelity in the interpolation between the dissimilar meshes for all cambers.

Acknowledgments

The VCCW project is a combined effort of various AFRL Aerospace Systems Directorate offices including, but not limited to Chris Marks, Lauren Zientarski, and Adam Culler, the FIRST lab, and the staff at the wind tunnel facility, without whom this effort would not have been successful.

References

[1]Joo, J., Marks, C., and Zeintarski, L., "AFRL Variable Camber Compliant Wing - Design," *SciTech 2015*, Kissimmee, FL, 2015.

[2]Farhat, C., van der Zee, K. G., and Geuzaine, P., "Provably second-order time-accurate loosely-coupled solution algorithms for transient nonlinear computational aeroelasticity," *Computer Methods in Applied Mechanics and Engineering*, Vol. 195, No. 17-18, March 2006, pp. 1973–2001.

[3]Farhat, C., Geuzaine, P., and Brown, G., "Application of a three-field nonlinear fluidstructure formulation to the prediction of the aeroelastic parameters of an F-16 fighter," *Computers & Fluids*, Vol. 32, No. 1, Jan. 2003, pp. 3–29.

[4]Degroote, J., "Partitioned Simulation of Fluid-Structure Interaction," *Archives of Computational Methods in Engineering*, Vol. 20, No. 3, July 2013, pp. 185–238.

[5]Zhao, X., Zhu, Y., and Zhang, S., "Transonic wing flutter predictions by a loosely-coupled method," *Computers & Fluids*, Vol. 58, April 2012, pp. 45–62.

[6]Zwaan, R. and Prananta, B., "Fluid/structure interaction in numerical aeroelastic simulation," *International Journal of Non-Linear Mechanics*, Vol. 37, No. 4-5, June 2002, pp. 987–1002.

[7]Mian, H. H., Wang, G., and Ye, Z.-Y., "Numerical investigation of structural geometric nonlinearity effect in high-aspect-ratio wing using CFD/CSD coupled approach," *Journal of Fluids and Structures*, Vol. 49, Aug. 2014, pp. 186–201.

[8]Biedron, R. T., Derlaga, J. M., Gnoffo, P. A., Hammond, D. P., Jones, W. T., Kleb, B., Lee-rausch, E. M., Nielsen, E. J., Park, M. A., Rumsey, C. L., Thomas, J. L., and Wood, W. A., *FUN3D Manual: 12.5*, No. September, NASA Langley Research Center, Hampton, VA, nasa/tm20 ed., 2014.

[9]Samareh, J. and Bhatia, K., "A unified approach to modeling multidisciplinary interactions," *8th Symposium on Multidisciplinary Analysis and Optimization*, Multidisciplinary Analysis Optimization Conferences, American Institute of Aeronautics and Astronautics, Sept. 2000.

[10]Samareh, J., "Discrete Data Transfer Technique for Fluid-Structure Interaction," *18th AIAA Computational Fluid Dynamics Conference*, Fluid Dynamics and Co-located Conferences, American Institute of Aeronautics and Astronautics, June 2007.

[11]Marks, C., Zeintarski, L., and Joo, J., "AFRL Variable Camber Compliant Wing - Wind Tunnel Testing," *SciTech 2015*, Kissimmee, FL, 2015.

[12]Spalart, P. R. and Allmaras, S. R., "A One-Equation Turblence Model for Aerodynamic Flows," *Recherche Aerospatiale*, Vol. 1, 1994, pp. 5–21.